The Astrophysical Journal, 769:92 (9pp), 2013 June 1 doi:10.1088/0004-637X/769/2/92


# ULTRA-LUMINOUS X-RAY SOURCES IN THE MOST METAL POOR GALAXIES

A. H. Prestwich[1], Maria Tsantaki[2,3], A. Zezas[1,2,4], F. Jackson[1], T. P. Roberts[5], R. Foltz[6], T. Linden[7], and V. Kalogera[8]
[1] Harvard-Smithsonian Center for Astrophysics, 60 Garden Street, Cambridge, MA 02138, USA
[2] Physics Department, University of Crete, 71003 Heraklion, Crete, Greece
[3] Centro de Astrofsica, Universidade do Porto, Rua das Estrelas, 4150-762 Porto, Portugal
[4] Foundation for Research and Technology-Hellas, 71110 Heraklion, Crete, Greece
[5] Department of Physics, University of Durham, South Road, Durham DH1 3LE, UK
[6] Department of Physics and Astronomy, University of California, Riverside, 900 University Avenue, Riverside, CA 92521, USA
[7] Department of Physics, University of Santa Cruz, 211 Interdisciplinary Sciences Building, 1156 High Street, Santa Cruz, CA 95064, USA
[8] Center for Interdisciplinary Exploration and Research in Astrophysics (CIERA) & Department of Physics and Astronomy, Northwestern University, 2145 Sheridan Road, Evanston, IL 60208, USA
*Received 2012 August 31; accepted 2013 February 6; published 2013 May 7*

## ABSTRACT

Ultra-luminous X-ray sources (ULX) are X-ray binaries with $L_x > 10^{39}$ erg s$^{-1}$. The most spectacular examples of ULX occur in starburst galaxies and are now understood to be young, luminous high mass X-ray binaries. The conditions under which ULX form are poorly understood, but recent evidence suggests they may be more common in low metallicity systems. Here we investigate the hypothesis that ULX form preferentially in low metallicity galaxies by searching for ULX in a sample of extremely metal poor galaxies (XMPG) observed with the *Chandra X-Ray Observatory*. XMPG are defined as galaxies with log(O/H) + 12 < 7.65, or less than 5% solar. These are the most metal-deficient galaxies known, and a logical place to find ULX if they favor metal poor systems. We compare the number of ULX (corrected for background contamination) per unit of star formation ($N_{\rm ULX}$(SFR)) in the XMPG sample with $N_{\rm ULX}$(SFR) in a comparison sample of galaxies with higher metallicities taken from the Spitzer Infrared Galaxy Sample. We find that ULX occur preferentially in the metal poor sample with a formal statistical significance of $2.3\sigma$. We do not see strong evidence for a trend in the formation of ULX in the high metallicity sample: above 12+log(O/H) $\sim$ 8.0 the efficiency of ULX production appears to be flat. The effect we see is strongest in the lowest metallicity bin. We discuss briefly the implications of these results for the formation of black holes in low metallicity gas.

*Key words:* stars: formation – X-rays: binaries

*Online-only material:* color figures

## 1. INTRODUCTION

Ultra-luminous X-ray sources (ULX) are X-ray binaries with $L_x > 10^{39}$ erg s$^{-1}$ most commonly found in star forming and starburst galaxies. These sources have attracted considerable attention in recent years because they have broadband X-ray luminosities many times the Eddington limit for a neutron star or stellar mass black hole (Miller & Colbert 2004; Roberts 2007; Feng & Soria 2011). Some of these extreme objects may be intermediate mass black holes ($M > 500\,M_\odot$; Colbert & Mushotzky 1999; Farrell et al. 2009; Sutton et al. 2012). It seems likely, however that most ULX are stellar X-ray sources which are either radiating in excess of the Eddington limit and/or have black-hole masses somewhat higher than is commonly seen in black hole candidates in Milky Way binaries ($M > 10\,M_\odot$; Roberts 2007; Gladstone et al. 2009; Zampieri & Roberts 2009). ULX are found in a wide variety of systems—spirals, interacting starbursts, and dwarf galaxies. However, the conditions under which ULX form are poorly understood.

It is well established that the number of ULX in star-forming galaxies scales with the star formation rate (SFR; Grimm et al. 2003; Ranalli et al. 2003; Mapelli et al. 2010; Mineo et al. 2012). In addition, there are several lines of evidence to suggest that ULX form preferentially in low metallicity gas. Kaaret et al. (2011) found that the ratio of X-ray luminosity to SFR is an order of magnitude larger in low metallicity blue compact dwarf galaxies than for solar metallicity star forming galaxies. Swartz et al. (2008) found that the occurrence rate per unit galaxy mass is higher in dwarfs than in more massive galaxies (see also Walton et al. 2011). This surprising correlation is explained if ULX favor the metal poor environments found in dwarfs. Evidence that there is a direct connection between metallicity and ULX production was presented by Mapelli et al. (2010) who find an anti-correlation between the number of ULX and metallicity based on a sample of 64 galaxies. A further study by Mapelli et al. (2011) with the addition of two XMPG came to the same conclusion. Spectroscopy of ULX counterparts and surrounding gas also suggest that ULX are formed from stars in metal poor gas (e.g., Soria et al. 2005; Liu et al. 2007).

Here we investigate the hypothesis that ULX form preferentially in low metallicity galaxies by searching for ULX in a sample of extremely metal poor galaxies (XMPG) observed with the *Chandra X-Ray Observatory*. XMPG are defined as galaxies with log(O/H) + 12 < 7.65, or less than 5% solar (Papaderos et al. 2008). These are the most metal-deficient galaxies known, and a logical place to find ULX if they favor metal poor systems. Our goal is to compare the number of ULX (normalized to the SFR and accounting for cosmic background sources) in a sample of XMPG with a comparison sample of galaxies with higher metallicities taken from the Spitzer Infrared Galaxy Sample (SINGS). For a sample of galaxies we define $N_{\rm ULX}$(SFR) to be

$$N_{\rm ULX}({\rm SFR}) = \frac{\sum N_{\rm ULX} - \sum N_{\rm BKG}}{\sum {\rm SFR}}. \quad (1)$$

**Table 1**
The Extremely Metal Poor Galaxy Sample

| Galaxy | R.A. (J2000) | Decl. (J2000) | Distance (Mpc) | $D_{25}$ (arcmin) | $N_{\rm H}$ ($10^{20}$ cm$^{-2}$) | 12+log(O/H) |
|---|---|---|---|---|---|---|
| UGC 772 | $08^{h}25^{m}55^{s}.5$ | $+35^{d}32^{m}32^{s}$ | 3.10 | $1.20 \times 0.90$ | 11.5 | $7.24 \pm 0.03$ |
| SDSS J210455.31−003522.2 | $21^{h}04^{m}55^{s}.3$ | $-00^{d}35^{m}22^{s}$ | 13.7 | ... | 6.47 | $7.26 \pm 0.03$ |
| SBS 1129+576 | $11^{h}32^{m}02^{s}.5$ | $+57^{d}22^{m}46^{s}$ | 26.3 | $0.75 \times 0.10$ | 0.87 | $7.41 \pm 0.07$ |
| HS 0822+3542 | $08^{d}25^{m}55^{s}.5$ | $+35^{d}32^{m}32^{s}$ | 12.7 | $0.27 \times 0.12$ | 4.82 | 7.35 |
| SDSS J120122.32+021108.5 | $12^{h}01^{m}22^{s}.3$ | $+02^{d}11^{m}08^{s}$ | 18.4 | $0.35 \times 0.12$ | 1.88 | $7.55 \pm 0.03$ |
| RC2 A1116+51 | $11^{h}19^{m}34^{s}.3$ | $+51^{d}30^{m}12^{s}$ | 20.8 | $0.24 \times 0.17$ | 1.19 | $7.51 \pm 0.04$ |
| SBS 0940+544 | $09^{h}44^{m}16^{s}.6$ | $+54^{d}11^{m}34^{s}$ | 24.7 | $1.22 \times 1.54$ | 1.34 | 7.48 |
| KUG 1013+381 | $10^{h}16^{m}24^{s}.5$ | $+37^{d}54^{m}46^{s}$ | 19.6 | $0.38 \times 0.25$ | 1.41 | 7.58 |
| SBS 1415+437 | $14^{h}17^{m}01^{s}.4$ | $+43^{d}30^{m}05^{s}$ | 10.4 | $0.75 \times 0.15$ | 1.21 | 7.60 |
| 6dF J0405204−364859 | $04^{h}05^{m}20^{s}.3$ | $-36^{d}49^{m}01^{s}$ | 11.0 | $0.48 \times 0.35$ | 0.88 | 7.34 |
| SDSS J141454.13−020822.9 | $14^{h}14^{m}54^{s}.1$ | $-02^{d}08^{m}23^{s}$ | 24.6 | $0.34 \times 0.24$ | 4.17 | 7.32 |
| SDSS J223036.79−000636.9 | $22^{h}30^{m}36^{s}.8$ | $-00^{d}06^{m}37^{s}$ | 18.0 | $0.24 \times 0.20$ | 5.20 | 7.64 |
| UGCA 292 | $12^{h}38^{m}40^{s}.0$ | $+32^{d}46^{m}01^{s}$ | 3.5 | $1.00 \times 0.70$ | 1.34 | $7.27 \pm 0.08$ |
| HS 1442+4250 | $14^{h}44^{m}12^{s}.8$ | $+42^{d}37^{m}44^{s}$ | 10.5 | $1.13 \times 0.26$ | 1.53 | 7.63 |
| KUG 0201−103 | $02^{h}04^{m}25^{s}.6$ | $-10^{d}09^{m}35^{s}$ | 22.7 | $0.46 \times 0.19$ | 2.08 | 7.56 |
| SDSS J081239.52+483645.3 | $08^{h}12^{m}39^{s}.5$ | $+48^{d}36^{m}45^{s}$ | 9.04 | $0.46 \times 0.23$ | 4.58 | 7.16 |
| SDSS J085946.92+392305.6 | $08^{h}59^{m}46^{s}.9$ | $+39^{d}23^{m}06^{s}$ | 10.9 | $0.39 \times 0.27$ | 2.44 | 7.45 |
| KUG 0743+513 | $07^{h}47^{m}32^{s}.1$ | $+51^{d}11^{m}28^{s}$ | 8.6 | $0.70 \times 0.30$ | 5.17 | 7.68 |
| KUG 0937+298 | $09^{h}40^{m}12^{s}.8$ | $+29^{d}35^{m}30^{s}$ | 11.2 | $0.62 \times 0.23$ | 1.87 | 7.45 |
| KUG 0942+551 | $09^{h}46^{m}22^{s}.8$ | $+54^{d}52^{m}08^{s}$ | 24.4 | $0.37 \times 0.18$ | 1.23 | 7.66 |
| SBS 1102+606 | $11^{h}05^{m}53^{s}.7$ | $+60^{d}22^{m}29^{s}$ | 19.9 | $0.60 \times 0.28$ | 0.59 | $7.64 \pm 0.04$ |
| RC2 A1228+12 | $12^{h}30^{m}48^{s}.5$ | $+12^{d}02^{m}42^{s}$ | 21.2 | $0.29 \times 0.16$ | 2.47 | 7.64 |
| I Zw 18 | $09^{h}34^{m}02^{s}.0$ | $+55^{d}14^{m}28^{s}$ | 17.1 | $0.30 \times 0.20$ | 1.99 | 7.17 |
| SBS 0335−052 | $03^{h}37^{m}44^{s}.0$ | $-05^{d}02^{m}40^{s}$ | 52.6 | $0.23 \times 0.20$ | 4.98 | $7.25 \pm 0.05$ |
| SBS 0335−052W | $03^{h}37^{m}38.4 \times$ s | $-05^{d}02^{m}37^{s}$ | 52.2 | $0.10 \times 0.13$ | 4.96 | $7.10 \pm 0.08$ |

**Notes.** Distances are taken from the NASA/IPAC Extragalactic Database (NED). $D_{25}$ shows the diameter of major×minor axis. The Galactic $N_{\rm H}$ is calculated with Colden tool, http://cxc.harvard.edu/toolkit/colden.jsp. Metallicities are taken from literature. For the galaxy SDSS J210455.31−003522.2 we used the optical diameter from NASA/SAO Image Archive.

Here $\sum N_{\rm ULX}$ is the total number of ULX found in a sample of galaxies (e.g., the XMPG sample), $\sum N_{\rm BKG}$ the total number of expected cosmic background sources (with an apparent luminosity $>10^{39}$ erg s$^{-1}$) in the same sample and $\sum$ SFR is the integrated SFR (in $M_{\odot}$ per year) of the sample galaxies.

## 2. GALAXY SAMPLE

Our sample is listed in Table 1. It consists of 25 nearby ($d \leqslant 50$ Mpc) XMPG ((O/H) + 12 < 7.65). These are the most metal-deficient galaxies known. Most of those are blue compact dwarf galaxies. Three galaxies in the sample (I Zw18, SBS 0335−052, SBS 0335−052W) were observed with *Chandra* in 2000 (Thuan et al. 2004). The remainder were observed as part of a Cycle 11 Large Project. The exposure times were set to obtain a $3.5\sigma$ detection of a point source of luminosity $7.8 \times 10^{38}$ erg cm$^{-2}$ s$^{-1}$ (i.e., our survey is complete down to $7.8 \times 10^{38}$ erg cm$^{-2}$ s$^{-1}$). Completeness is further discussed in Section 3.1. Observational details are given in Table 2.

## 3. X-RAY OBSERVATIONS

All observations were obtained with the back-illuminated chip ACIS-S3 except for the galaxies SBS 0335−052 and SBS 0335−052W, which were observed with the front-illuminated ACIS-I3 camera. The observations were performed in VFAINT mode. We reprocessed raw data (level 1 event files) using Chandra Interactive Analysis of Observations software (CIAO), version 4.2 and the CALibration DataBase (CALDB), version 4.3.0. Standard routines were used to correct for bad pixels, charge transfer inefficiency and time dependent gain. A new Level 2 events file was created by filtering for standard grades (0, 2, 3, 4, 6) and rejecting grades associated with bad pixels.

The positions of X-ray sources were determined with the CIAO tool WAVDETECT. This tool is a wavelet-based source detection algorithm (Freeman et al. 2002). The X-ray image is convolved with a wavelet function to produce a "correlation image." Clumps of counts (sources) are identified as a local maximum in the correlation image if the scale of the wavelet is approximately equal to (or greater than) the size of the clump. Hence, WAVDETECT also gives an estimate of the size of the source. It is typically run with wavelets of differing scales to better detect extended emission.

WAVDETECT was run on the level 2 files in the 0.3–8 keV band using scales of 1.0, 2.0, 4.0, 8.0, and 16.0 pixels. We set a threshold significance for identifying a pixel as belonging to the source at $10^{-6}$. All the detected sources have scales consistent with their being point sources. Sources within the $D_{25}$ region (defined as the elliptical contour best corresponding to the 25 mag arcsec$^{-2}$ blue isophote; de Vaucouleurs et al. 1991) were considered to be associated with the galaxy. The results of the source detection are show in Table 3.

Source regions were defined based on the WAVDETECT source extent. We also create the corresponding background regions by setting apertures with larger radii than the sources. We perform photometry for these sources, using the `dmextract` tool. The results of the photometry are shown at Table 5. The source counts per pixel follow the Poisson distribution and the count error, since the number of counts is very low, the Gehrels approximation: error $= 1 + \sqrt{(N + 0.75)}$ (Gehrels 1986).

The flux of an X-ray source is proportional to the net count rate, where the constant of proportionality depends on the

**Table 2**
X-Ray Observations

| Galaxy | ObsID | Date | Exposure (s) | Instrument |
|---|---|---|---|---|
| UGC 772 | 11281 | 2009 Aug 30 | 5081 | ACIS-S3 |
| SDSS J210455.31−003522.2 | 11282 | 2009 Sep 4 | 5007 | ACIS-S3 |
| SBS 1129+576 | 11283 | 2010 Jul 6 | 14755 | ACIS-S3 |
| HS 0822+3542 | 11284 | 2009 Dec 20 | 51200 | ACIS-S3 |
| SDSS J120122.32+021108.5 | 11286 | 2009 Nov 23 | 8097 | ACIS-S3 |
| RC2 A1116+51 | 11287 | 2009 Nov 7 | 11640 | ACIS-S3 |
| SBS 0940+544 | 11288 | 2010 Jan 18 | 16828 | ACIS-S3 |
| KUG 1013+381 | 11289 | 2010 Jan 24 | 9402 | ACIS-S3 |
| SBS 1415+437 | 11291 | 2009 Oct 30 | 5114 | ACIS-S3 |
| 6dF J0405204−364859 | 11292 | 2010 May 28 | 5010 | ACIS-S3 |
| SDSS J141454.13−020822.9 | 11293 | 2009 Dec 18 | 16680 | ACIS-S3 |
| SDSS J223036.79−000636.9 | 11294 | 2009 Sep 25 | 7715 | ACIS-S3 |
| UGCA 292 | 11295 | 2009 Nov 6 | 5007 | ACIS-S3 |
| HS 1442+4250 | 11296 | 2009 Nov 26 | 5188 | ACIS-S3 |
| KUG 0201−103 | 11297 | 2009 Sep 6 | 13590 | ACIS-S3 |
| SDSS J081239.52+483645.3 | 11298 | 2009 Dec 18 | 4777 | ACIS-S3 |
| SDSS J085946.92+392305.6 | 11299 | 2009 Dec 18 | 4782 | ACIS-S3 |
| KUG 0743+513 | 11300 | 2009 Dec 18 | 5073 | ACIS-S3 |
| KUG 0937+298 | 11301 | 2010 Jan 16 | 5007 | ACIS-S3 |
| KUG 0942+551 | 11302 | 2010 Jan 19 | 16020 | ACIS-S3 |
| SBS 1102+606 | 11285 | 2010 Aug 23 | 10340 | ACIS-S3 |
| RC2 A1228+12 | 11290 | 2010 Jul 26 | 12200 | ACIS-S3 |
| I Zw 18 | 805 | 2000 Feb 8 | 40750 | ACIS-S3 |
| SBS 0335−052 | 796 | 2000 Sep 7 | 59742 | ACIS-I3 |
| SBS 0335−052W | 796 | 2000 Sep 7 | 59742 | ACIS-I3 |

**Table 3**
X-Ray Source Detection

| Galaxy | Number of Sources | Position R.A. (J2000) Decl. (J2000) |
|---|---|---|
| SBS 1129+576 | 1 | $11^h32^m02^s.57$ $+57^d22^m36^s.87$ |
| RC2 A1116+51 | 1 | $11^h19^m34^s.13$ $+51^d30^m12^s.48$ |
| SBS 0940+544 | 1 | $09^h44^m16^s.44$ $+54^d11^m34^s.39$ |
| I ZW 18 | 1 | $09^h34^m01^s.97$ $+55^d14^m28^s.23$ |
| SBS 0335−052 | 1 | $03^h37^m44^s.04$ $-05^d02^m39^s.89$ |
| SBS 0335−052W | 1 | $03^h37^m38^s.44$ $-05^d02^m37^s.14$ |

**Table 4**
Spectral Fit to I ZW 18

| Galaxy | Source Count-rate (counts $s^{-1}$) | $\Gamma$ | $N_H$ ($10^{20}$ $cm^{-2}$) | $\chi^2$/dof |
|---|---|---|---|---|
| I ZW 18 | 0.0111 | $1.88^{+0.22}_{-0.20}$ | $7.54^{+4.76}_{-6.17}$ | 12.69/19 |

response of the detector and the assumed source spectrum:

$$A = \frac{\text{Flux}}{\text{Count Rate}}\ [(\text{erg s}^{-1}\ \text{cm}^{-2})/(\text{counts s}^{-1})]. \quad (2)$$

We extracted standard spectral responses (the Redistribution Matrix (RMF) and Area Response Matrix) and simulated a spectrum for each source. Using the results of Swartz et al. (2004), we adopt an intrinsic source spectrum with photon index $\Gamma = 1.7$ and assume values for galactic absorption taken from Dickey & Lockman (1990). We then estimate the constant A from the ratio of the number of counts to the calculated flux in the simulated spectrum. Fluxes and luminosities were constructed in the 0.3–8 keV band, using the constant $A$ derived from the simulated spectra. They are shown in Table 5. One source, IZw18, had enough counts to perform a spectral fit. The best fit is consistent with the analysis of Thuan et al. (2004) and is shown in Table 4. The fluxes and luminosities of the other sources are shown in Table 5.

### 3.1. Completeness and Background Sources

In this section we demonstrate that our sample of ULX in the metal-poor galaxies is complete: i.e., that we are not "missing" ULX due to inadequate exposure. In addition, we estimate the number of ULX which are chance coincidences: background active galactic nucleus (AGN) that happen to align with the optical galaxy.

The completeness limit is expressed by the source detection probability of a galaxy. It is a function of the source and background intensity, measured in counts. The detection probability as a function of source counts and background counts/pixel can be parameterized by the following function (Zezas et al. 2007):

$$A(C) = 1.0 - \lambda_0 C^{-\lambda_1} e^{-\lambda_2 C} \quad (3)$$

where $C$ is the source intensity in counts, $\lambda_0$, $\lambda_1$, $\lambda_2$ parameters that depend on the background counts per pixel.

All galaxies of our sample were measured to have background level below 0.025 counts per pixel. The best-fit parameters for this background give a detection probability of the form:

$$A(C) = 1.0 - 11.12C^{-0.83} e^{-0.43C}. \quad (4)$$

Therefore, by solving the equation for 90% and 50% completeness, the corresponding source counts are $C_{90} = 7.2$ counts and $C_{50} = 4.4$ counts.

Table 6 shows that all luminosities of 90% completeness and all luminosities 50% completeness, are well under the limit of $10^{39}$ erg $s^{-1}$ $cm^2$. This means that we have detected at least 90% of all existing ULX sources in the galaxy sample.

**Table 5**
X-Ray Photometry

| Galaxy | Net Counts | Background Counts | $N_H$ ($10^{20} F$ cm$^{-2}$) | Flux ($10^{-15}$ erg cm$^{-2}$ s$^{-1}$) | $L_x$ ($10^{39}$ erg s$^{-1}$) |
|---|---|---|---|---|---|
| SBS 1129+576 | 21.47 ± 5.71 | 0.19 ± 1.97 | 0.87 | 1.14 ± 0.3 | 0.72 ± 0.19 |
| RC2 A1116+51 | 89.04 ± 10.48 | 0.21 ± 1.98 | 1.19 | 5.95 ± 0.70 | 2.93 ± 0.35 |
| SBS 0940+544 | 39.20 ± 7.32 | 0.20 ± 1.97 | 1.34 | 1.81 ± 0.34 | 1.26 ± 0.24 |
| I ZW 18 | 494.44 ± 23.25 | 1.56 ± 2.51 | 7.54 | 7.46 ± 0.35 | 4.92 ± 0.25 |
| SBS 0335−052 | 28.21 ± 6.38 | 1.30 ± 2.43 | 4.98 | 0.56 ± 0.13 | 1.86 ± 0.42 |
| SBS 0335−052W | 116.29 ± 11.82 | 1.30 ± 2.43 | 4.96 | 2.31 ± 0.23 | 7.53 ± 0.77 |

**Table 6**
Completeness

| Galaxy | Exposure Time (s) | 90% ($10^{38}$ erg s$^{-1}$) | 50% ($10^{38}$ erg s$^{-1}$) | $N_{BKG}$ |
|---|---|---|---|---|
| UGC 772 | 5081 | 1.66 | 1.01 | 0.014 |
| SDSS J210455.31−003522.2 | 5007 | 2.39 | 1.46 | 0.039 |
| SBS 1129+576 | 14755 | 2.40 | 1.47 | 0.034 |
| HS 0822+3542 | 5120 | 2.00 | 1.23 | 0.004 |
| SDSS J120122.32+021108.5 | 8097 | 2.66 | 1.63 | 0.010 |
| RC2 A1116+51 | 11640 | 2.37 | 1.45 | 0.012 |
| SBS 0940+544 | 16828 | 2.31 | 1.41 | 0.776 |
| KUG 1013+381 | 9402 | 2.60 | 1.59 | 0.026 |
| SBS 1415+437 | 5114 | 1.35 | 0.82 | 0.010 |
| 6dF J0405204−364859 | 5010 | 1.54 | 0.94 | 0.017 |
| SDSS J141454.13−020822.9 | 16680 | 2.31 | 1.41 | 0.034 |
| SDSS J223036.79−000636.9 | 7715 | 2.67 | 1.63 | 0.012 |
| UGCA 292 | 5007 | 0.08 | 0.05 | 0.041 |
| HS 1442+4250 | 5188 | 1.35 | 0.83 | 0.028 |
| KUG 0201−103 | 13590 | 2.41 | 1.47 | 0.031 |
| SDSS J081239.52+483645.3 | 4777 | 1.09 | 0.67 | 0.008 |
| SDSS J085946.92+392305.6 | 4782 | 1.58 | 0.97 | 0.011 |
| KUG 0743+513 | 5073 | 0.93 | 0.57 | 0.014 |
| KUG 0937+298 | 5007 | 1.59 | 0.97 | 0.015 |
| KUG 0942+551 | 16020 | 2.36 | 1.45 | 0.027 |
| SBS 1102+606 | 10340 | 2.44 | 1.49 | 0.048 |
| RC2 A1228+12 | 12200 | 2.37 | 1.43 | 0.014 |
| I ZW 18 | 25956 | 0.72 | 0.44 | 0.013 |
| SBS 0335−052 | 59742 | 4.74 | 2.89 | 0.070 |
| SBS 0335−052W | 59742 | 4.66 | 2.85 | 0.020 |

The predicted number of background sources for each galaxy was estimated as follows. For each galaxy, we calculate the 0.3–8 keV flux for a source of $10^{39}$ erg s$^{-1}$ and then transform the flux to the 0.5–2 keV band assuming a power law source spectrum with photon index $\Gamma = 1.7$ and a foreground $N_H$ listed in Table 1. We then used the log $N$–log $S$ curves of Giacconi et al. (2001) for the 0.5–2 keV band to estimate the number of background sources per square degree and normalize by the $D_{25}$ values to get the absolute number of background sources predicted to lie within the optical area of the galaxy. These values are given in Table 6. We note that SBS 0940+544 has a predicted background value close to one.

## 4. ESTIMATES OF THE STAR FORMATION RATE IN THE XMPG SAMPLE

It is well established that the number of ULX in a galaxy scales with the SFR (Grimm et al. 2003; Ranalli et al. 2003; Mapelli et al. 2010; Mineo et al. 2012). We therefore need reliable estimates of the SFR in the XMPG sample in order to determine whether $N_{ULX}$(SFR) is higher in the metal poor sample than in the SINGS sample. We use two methods to estimate the SFR: the far-ultraviolet (FUV) luminosity from *Galaxy Evolution Explorer* (*GALEX*) and the 24 $\mu$m luminosity from *Spitzer*.

### 4.1. GALEX Data

The FUV emission from star forming regions comes directly from young massive O and B stars. We use the method from Hunter et al. (2010) to relate the FUV luminosity to the SFR in dwarf galaxies:

$$\mathrm{SFR_{FUV}}(M_\odot\ \mathrm{yr}^{-1}) = 1.27 \times 10^{-28}\, L_{\mathrm{FUV}}\,(\mathrm{erg\ s^{-1}\ Hz^{-1}}). \quad (5)$$

We obtained *GALEX* FUV images from the GalexView version 1.4.6 catalog. All galaxies in the XMPG sample were detected with the exception of SDSS J223036.79−000636.9. This galaxy is excluded from the rest of the analysis in this paper. Source counts were extracted using the *CIAO* DMEXTRACT routine. This was done with either circular or elliptical source apertures, depending on the morphology of the galaxy in question, as well as an annular background aperture. Both of these apertures were centered on the source, with the circular apertures having a radius of either 10 or 15 pixels, and the ellipses having a semi-major and semi-minor axis of length 28 and 14 pixels or 15 and 7.5 pixels, respectively, depending on the

**Table 7**
UV Measurements and SFRs

| Galaxy | $E(B-V)$[a] (mag) | Count Rate[b] (counts $s^{-1}$) | $L_{FUV}$[c] ($\times 10^{26}$ erg $s^{-1}$ $Hz^{-1}$) | $SFR_{FUV}$[d] ($10^{-3}$ $M_\odot$ $yr^{-1}$) |
|---|---|---|---|---|
| UGC 772 | 0.028 | $5.55 \pm 0.05$ | $0.09 \pm 0.001$ | $1.09 \pm 0.01$ |
| SDSS J210455.31−003522.2 | 0.066 | $1.21 \pm 0.06$ | $0.49 \pm 0.02$ | $6.22 \pm 0.29$ |
| SBS 1129+576 | 0.013 | $3.48 \pm 0.20$ | $3.47 \pm 0.20$ | $44.02 \pm 2.52$ |
| HS 0822+3542 | 0.047 | $1.08 \pm 0.09$ | $0.32 \pm 0.03$ | $4.11 \pm 0.33$ |
| SDSS J120122.32+021108.5 | 0.024 | $1.20 \pm 0.03$ | $0.64 \pm 0.02$ | $8.07 \pm 0.20$ |
| RC2 A1116+51 | 0.015 | $4.38 \pm 0.21$ | $2.58 \pm 0.12$ | $32.76 \pm 1.57$ |
| SBS 0940+544 | 0.013 | $1.56 \pm 0.11$ | $1.37 \pm 0.10$ | $17.41 \pm 1.25$ |
| KUG 1013+381 | 0.015 | $7.63 \pm 0.26$ | $4.24 \pm 0.15$ | $53.87 \pm 1.87$ |
| SBS 1415+437 | 0.009 | $12.69 \pm 0.30$ | $1.93 \pm 0.05$ | $24.55 \pm 0.59$ |
| 6dF J0405204−364859 | 0.006 | $5.29 \pm 0.22$ | $0.80 \pm 0.03$ | $10.12 \pm 0.43$ |
| SDSS J141454.13−020822.9 | 0.058 | $0.63 \pm 0.02$ | $0.78 \pm 0.02$ | $9.88 \pm 0.30$ |
| UGCA 292 | 0.016 | $7.15 \pm 0.18$ | $0.13 \pm 0.003$ | $1.62 \pm 0.04$ |
| HS 1442+4250 | 0.013 | $9.00 \pm 0.22$ | $1.42 \pm 0.04$ | $18.08 \pm 0.45$ |
| KUG 0201−103 | 0.021 | $1.30 \pm 0.09$ | $1.02 \pm 0.07$ | $13.00 \pm 0.87$ |
| SDSS J081239.52+483645.3 | 0.051 | $0.86 \pm 0.02$ | $0.13 \pm 0.003$ | $1.71 \pm 0.04$ |
| SDSS J085946.92+392305.6 | 0.026 | $0.71 \pm 0.01$ | $0.14 \pm 0.001$ | $1.72 \pm 0.02$ |
| KUG 0743+513 | 0.070 | $12.58 \pm 0.34$ | $1.66 \pm 0.04$ | $21.12 \pm 0.57$ |
| KUG 0937+298 | 0.018 | $5.21 \pm 0.16$ | $0.97 \pm 0.03$ | $12.34 \pm 0.37$ |
| KUG 0942+551 | 0.012 | $1.48 \pm 0.12$ | $1.26 \pm 0.10$ | $16.01 \pm 1.27$ |
| SBS 1102+606 | 0.006 | $4.19 \pm 0.17$ | $2.27 \pm 0.09$ | $28.79 \pm 1.14$ |
| RC2 A1228+12 | 0.027 | $2.69 \pm 0.04$ | $2.03 \pm 0.03$ | $25.69 \pm 0.39$ |
| I ZW18 | 0.032 | $11.52 \pm 0.08$ | $5.60 \pm 0.04$ | $71.12 \pm 0.52$ |
| SBS 0335−052 | 0.047 | $5.52 \pm 0.20$ | $28.41 \pm 1.00$ | $360.86 \pm 12.76$ |
| SBS 0335−052W | 0.046 | $0.56 \pm 0.01$ | $2.84 \pm 0.04$ | $36.07 \pm 0.53$ |

**Notes.**
[a] Reddening magnitude of the source, used to calculate source extinction.
[b] Observed background-subtracted source count rate.
[c] Extinction-corrected far-UV luminosity of the source.
[d] Star formation rate, calculated using the formula from Hunter et al. (2010).

size of the source. All background annuli had an area 8 times that of their respective source apertures. The fluxes were computed using the relationship $f_{FUV} = (1.4 \times 10^{-15}) \times$ count rate.[9] Note that these fluxes are in units of erg $cm^{-2}$ $s^{-1}$ $Å^{-1}$. We converted these values to units of erg $cm^{-2}$ $s^{-1}$ $Hz^{-1}$ by multiplying them by $\lambda^2/c$, where $\lambda$ is the effective wavelength of the FUV detector ($= 1528$ Å) and $c$ is the speed of light in units of Å $s^{-1}$. With the fluxes in these new units, we proceeded to calculate the $L_{FUV}$ values of the sources, which were subsequently corrected for extinction. We then calculated the $SFR_{FUV}$ estimates of the galaxies using the extinction-corrected luminosities; these values are shown in Table 7.

### 4.2. Spitzer Data

The 24 $\mu$m emission in galaxies comes from single photon transient heating of small grains and can be used as a tracer of recent star formation. Calzetti et al. (2007) derived the following relation between the SFR and 24 $\mu$m emission from calibrating H II regions in nearby galaxies:

$$SFR_{IR}(M_\odot\ yr^{-1}) = 1.31 \times 10^{-38}[L_{24\,\mu m}(erg\ s^{-1})]^{0.885}, \quad (6)$$

where for intermediate luminosity galaxies:

$$1 \times 10^{40} < L_{24\,\mu m} < 3 \times 10^{44}\ erg\ s^{-1}.$$

We acquired data from the *Spitzer Space Telescope* that were obtained with the MIPS instrument in the 24 $\mu$m band. We obtained the post-BCD (post Basic Calibrated Data) data for the nine galaxies in the sample that have available MIPS 24 $\mu$m data. The data sets consist of several exposures that are interpolated into one mosaic image. From these images we measure the surface brightness in units of MJy $sr^{-1}$. The post-BCD product mosaic pixel sizes are $2.42 \times 2.45$ $arcsec^2$ for the 24 $\mu$m detector.

We perform aperture photometry using funtools. We define an aperture for the source with an ellipse that includes the total flux of the source and an elliptical annulus for the background region. In order to calculate the total flux density of each source, we sum the total flux of the source, subtract the background, on a set of pixels and multiply by the number of steradian per pixel. We convert the surface brightness to the flux density with the following formula:

$$f_v = \sum_{\text{pixels}} 2.45 \times 2.45 \frac{\text{arcsec}^2}{\text{pixel}} \times 0.023504 \frac{\text{Flux}}{\text{arcsec}^2}(\text{mJy}). \quad (7)$$

The flux density is converted to monochromatic flux:

$$F = \frac{c}{\lambda} f_v(\lambda). \quad (8)$$

The uncertainty on the flux is calculated from the mosaic variance image by adding in quadrature the uncertainty of all pixels within the source aperture. The results are listed at Table 8.

[9] http://galexgi.gsfc.nasa.gov/docs/galex/FAQ/counts_background.html

**Table 8**
24 $\mu$m Measurements and SFRs

| Galaxy | Flux Density (mJy) | Flux ($10^{-13}$ erg s$^{-1}$ cm$^{-2}$) | $L_{24}$ ($10^{40}$ erg s$^{-1}$) | SFR ($M_\odot$ yr$^{-1}$) |
|---|---|---|---|---|
| HS 0822+3542 | $2.23 \pm 0.09$ | $2.78 \pm 0.12$ | $0.54 \pm 0.02$ | $0.002 \pm 0.001$ |
| SBS 0940+544 | $1.60 \pm 0.10$ | $2.01 \pm 0.13$ | $1.47 \pm 0.09$ | $0.005 \pm 0.003$ |
| KUG 1013+381 | $14.54 \pm 0.17$ | $18.2 \pm 0.21$ | $8.37 \pm 0.09$ | $0.022 \pm 0.002$ |
| SBS 1415+437 | $16.67 \pm 0.15$ | $20.8 \pm 0.19$ | $2.70 \pm 0.02$ | $0.008 \pm 0.001$ |
| UGCA 292 | $<0.87 \pm 0.31$ | $1.09 \pm 0.34$ | $0.08 \pm 0.03$ | $0.0003 \pm 0.0010$ |
| HS 1442+4250 | $3.23 \pm 0.11$ | $4.03 \pm 0.14$ | $0.53 \pm 0.02$ | $0.002 \pm 0.001$ |
| SBS 1102+606 | $1.33 \pm 0.10$ | $1.67 \pm 0.11$ | $0.79 \pm 0.06$ | $0.003 \pm 0.002$ |
| I Zw 18 | $4.84 \pm 0.11$ | $6.05 \pm 0.14$ | $2.12 \pm 0.05$ | $0.006 \pm 0.001$ |
| SBS 0335−052 | $67.25 \pm 0.20$ | $84.10 \pm 0.25$ | $278.94 \pm 0.84$ | $0.480 \pm 0.013$ |
| SBS 0335−052W | $0.14 \pm 0.04$ | $0.018 \pm 0.005$ | $0.58 \pm 0.17$ | $0.002 \pm 0.005$ |

**Notes.** The SFR errors were calculated with error propagation. For the galaxy UGCA 292 we calculate the upper limits.

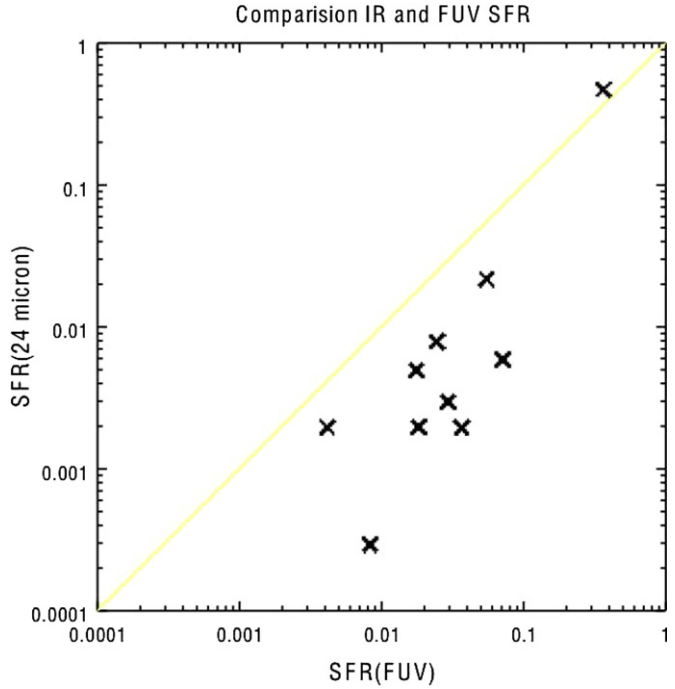


**Figure 1.** Comparison of the SFR determined from the FUV luminosity and 24 $\mu$m luminosity. The line denotes $SFR_{IR} = SFR_{FUV}$.
(A color version of this figure is available in the online journal.)

### 4.3. Comparison of Spitzer and GALEX Star Formation Rates

Several galaxies in the XMPG sample have both *GALEX* UV images and *Spitzer* 24 $\mu$m data. It is therefore instructive to compare SFR derived from the two methods. Figure 1 shows the SFR derived from the FUV flux with the SFR derived from the 24 $\mu$m flux. There is a clear correlation between the two methods. The rate derived from the FUV flux is systematically higher than for the 24 $\mu$m flux. This is almost certainly because 24 $\mu$m emission underestimates the SFR because of the very low dust content of the XMPG. We adopt the *GALEX* derived SFR because (1) the *Spitzer* 24 $\mu$m data likely underestimates the SFR, and (2) it is available for all the galaxies. We note that SBS 0335−052 appears to have very high SFR in comparison with the other XMPGs.

## 5. THE SINGS SAMPLE

In order to determine whether there is a statistically significant excess of ULX in the most metal poor systems, we require a comparison sample of galaxies with well determined SFRs and metallicities. The Spitzer Infrared Nearby Galaxies Survey (Kennicutt et al. 2003) is ideal for this purpose. It is a comprehensive imaging and spectroscopic study of 75 nearby galaxies with distances <30 Mpc. The morphological types of the sample range from elliptical to irregular. The SINGS sample does not include absolute extremes in properties that can be found in larger volumes such as ULIRGs, luminous AGNs or XMPG. A distance-limited sample of the SINGS survey has been observed by *Chandra* (L. Jenkins et al., in preparation). We use a sub-sample of SINGS galaxies selected by Calzetti et al. (2007) which have *Hubble Space Telescope* NICMOS images in the Pa$\alpha$ hydrogen emission line (1.8756 $\mu$m), H$\alpha$ observations and *Chandra* observations. The H$\alpha$ and the Pa$\alpha$ lines are used to measure the extinction correction. Furthermore, the Pa$\alpha$ line is used to calibrate the mid-infrared emission. There are 33 galaxies in the Calzetti et al. (2007) sample, 26 of which also form part of the *Chandra* survey. The galaxies are divided into three groups according to their oxygen abundance: high-metallicity galaxies [12+log(O/H) $\geqslant$ 8.35], intermediate-metallicity galaxies [8.00 < 12+log(O/H) $\leqslant$ 8.35], and low-metallicity galaxies [12+log(O/H) $\leqslant$ 8.00]. For reference, the XMPGs have metallicities 12+log(O/H) $\leqslant$ 7.65. We list the main characteristics of the SINGS sample in Table 9.

The metallicities given in Table 9 are given as an upper and lower bound and taken from Moustakas et al. (2010). The lower bound is the metallicity derived using the calibration of Pilyugin & Thuan (2005, hereafter PT05) and the upper bound using the calibration of Kobulnicky & Kewley (2004, hereafter KK04). As discussed in Moustakas et al. (2010), the PT05 calibration is based on empirical abundance measurements of individual H II regions and the KK04 calibration on photoionization model calculations. The KK04 calibration gives abundances that are systematically higher than PT05. In this paper we choose the PT05 calibration since this method was used to derive the XMPG abundances. The results of this paper are unchanged if we use KK04 or an average of the two.

We estimate the SFR of the SINGS galaxies using the calibration of Calzetti et al. (2010):

$$\mathrm{SFR}(M_\odot\ \mathrm{yr}^{-1}) = 5.5 \times 10^{-42} \times [L(\mathrm{H}\alpha)_{\mathrm{obs}} + 0.02\, L(24\,\mu\mathrm{m})]. \quad (9)$$

Note that the $L(\mathrm{H}\alpha)_{\mathrm{obs}}$ is the observed H$\alpha$ luminosity without correction for internal dust attenuation.

We use the measurements of the H$\alpha$ and 24 $\mu$m fluxes of Dale et al. (2007) and Kennicutt et al. (2008, 2009). The numbers of

**Table 9**
Characteristics of the SINGS Sample

| Galaxy | Morphology | Distance (Mpc) | 12+log(O/H) | $L(H\alpha)_{obs}$ ($10^{40}$ erg s$^{-1}$) | SFR ($M_\odot$ yr$^{-1}$) | $N_{ULX}$ | $N_{BKG}$ |
|---|---|---|---|---|---|---|---|
| | | | High-metallicity Galaxies | | | | |
| NGC 0925 | SAB(s)d | 9.12 | 8.24–8.78 | 6.01 | 1.634 | 1 | 0.566 |
| NGC 2403 | SAB(s)cd | 3.5 | 8.31–8.81 | 5.12 | 1.225 | 1 | 0.474 |
| NGC 2841 | SA(r)b | 9.8 | 8.52–9.19 | 3.39 | 3.17 | 2 | 0.282 |
| NGC 2976 | SAc | 3.5 | 8.30–8.98 | 0.87 | 0.334 | 0 | 0.028 |
| NGC 3184 | SAB(rs)cd | 11.10 | 8.48–9.14 | 7.36 | 3.31 | 2 | 0.628 |
| NGC 3198 | SB(rs)c | 13.68 | 8.32–8.87 | 6.85 | 3.71 | 1 | 0.493 |
| NGC 3351 | SB(r)b | 10.1 | 8.60–9.22 | 3.71 | 3.907 | 0 | 0.093 |
| NGC 3627 | SAB(s)b | 8.7 | 8.49–9.10 | 10.9 | 11.362 | 2 | 0.312 |
| NGC 4559 | SAB(rs)cd | 11.1 | 8.25–8.79 | 10.6 | 2.545 | 3 | 0.578 |
| NGC 4569 | SAB(rs)ab | 16.58 | 8.56–9.19 | 4.84 | 6.731 | 1 | 1.015 |
| NGC 4625 | SAB(rs)m | 9.17 | 8.27–9.04 | 0.61 | 0.215 | 0 | 0.013 |
| NGC 4736 | (R)SA(r)ab | 5.3 | 8.31–9.01 | 3.45 | 2.709 | 3 | 0.357 |
| NGC 4826 | (R)SA(rs)ab | 5.6 | 8.59–9.2 | 4 4.05 | 2.732 | 0 | 0.209 |
| NGC 5055 | SA(rs)bc | 7.82 | 8.42–9.13 | 7.71 | 6.172 | 2 | 0.613 |
| NGC 5194 | SA(s)bc | 8.2 | 8.54–9.18 | 20.10 | 15.847 | 3 | 0.569 |
| NGC 6946 | SAB(rs)cd | 5.0 | 8.40–9.04 | 16.5 | 16.437 | 1 | 0.4258 |
| NGC 7331 | SA(s)b | 15.1 | 8.40–9.05 | 13.4 | 15.893 | 3 | 0.850 |
| | | | Intermediate-metallicity Galaxies | | | | |
| NGC 1705 | SA0- | 5.1 | 8.20–8.43 | 0.9 | 0.075 | 0 | 0.009 |
| IC 2574 | SAB(s)m | 2.8 | 7.94–8.26 | 0.97 | 0.128 | 0 | 0.084 |
| NGC 4236 | SB(s)dm | 4.45 | 8.07–8.56 | 1.3 | 0.183 | 0 | 0.411 |
| IC 4710 | SB(s)m | 7.8 | 8.11–8.62 | 1.6 | 0.231 | 1 | 0.071 |
| NGC 6822 | IB(s)m | 0.47 | 8.04–8.67 | 0.07 | 0.015 | 0 | 0.013 |
| | | | Low-metallicity Galaxies | | | | |
| Ho II | Im | 3.5 | 7.68–8.07 | 0.64 | 0.073 | 1 | 0.087 |
| DDO 053 | Im | 3.56 | 7.77–8.13 | 0.08 | 0.011 | 0 | 0.003 |
| Ho IX | Im | 3.3 | 7.61–7.98 | 0.01 | 0.009 | 1 | 0.008 |
| NGC 5408 | IB(s)m | 4.8 | 7.81–8.23 | 1.16 | 0.023 | 1 | 0.004 |

**Notes.** Galaxy morphologies are from the NASA/IPAC Extragalactic Database (NED). Adopted distances as derived by Masters (2005). Oxygen abundances are from Moustakas et al. (2010).

**Table 10**
Comparison of the SINGS and XMPGs Sample

| | High | Intermediate | Low | XMPGs | Low + XMPG |
|---|---|---|---|---|---|
| $\sum N_{ULX}$ | 25 | 1 | 3 | 5 | 8 |
| $\sum N_{BKG}$ | 7.5 | 0.6 | 0.1 | 1.3 | 1.4 |
| $N_{ULX}$(SFR) | $0.17 \pm 0.042$ | $0.65 \pm 1.0$ | $25.0 \pm 14.6$ | $4.5 \pm 2.3$ | $7.0 \pm 2.7$ |

ULX for the SINGS sample have been provided by *Chandra* SINGS team (L. Jenkins et al., in preparation).

## 6. COMPARISON BETWEEN THE SINGS AND XMPGs SAMPLES

In this section, we investigate the relationship between metallicity and $N_{ULX}$(SFR). Table 10 compares $N_{ULX}$(SFR) for the XMPG sample and the SINGS sample. The SINGS sample is divided into three sub-groups according to metallicity values (High, Intermediate and Low metallicity). In addition, we show $N_{ULX}$(SFR) obtained by combining the SINGS low metallicity sample and the XMPG sample. The difference in $N_{ULX}$(SFR) between the high metallicity SINGS galaxies and the low metallicity galaxies (comprising the XMPG and low metallicity SINGS galaxies) is $2.3\sigma$. The low metallicity sample has a small number of individual galaxies with very high $N_{ULX}$/SFR values (these have low SFR and one ULX). A Kolmogorov–Smirnov (K-S) test gives the probability that the two distributions (low metallicity and SINGS) come from the same parent population as 0.18. Finally, Figure 2 shows $N_{ULX}$(SFR) as a function of metallicity. The high metallicity SINGS galaxies are plotted as individual points, and the XMPG and SINGS low metallicity galaxies are combined. We note that for galaxies with no ULX, the background-subtracted number of ULX is negative, which is unphysical. There is a marked increase in $N_{ULX}$(SFR) in the low metallicity galaxies. We conclude that ULX form preferentially in low metal systems, with the caveat that the formal significance of this result is low.

We do not find any evidence for a trend in $N_{ULX}$(SFR) with metallicity 12+log(O/H) $> 8.0$. Fitting the data points in Figure 2 above 12+log(O/H) $= 8.0$ with both a flat line (slope 0) and a straight line with non-zero slope we find that the more complex model (non-zero slope) is slightly preferred on the basis of a $\chi^2$ fit. We use an $F$-test to determine whether the model with a slope is significantly better than the flat line (the

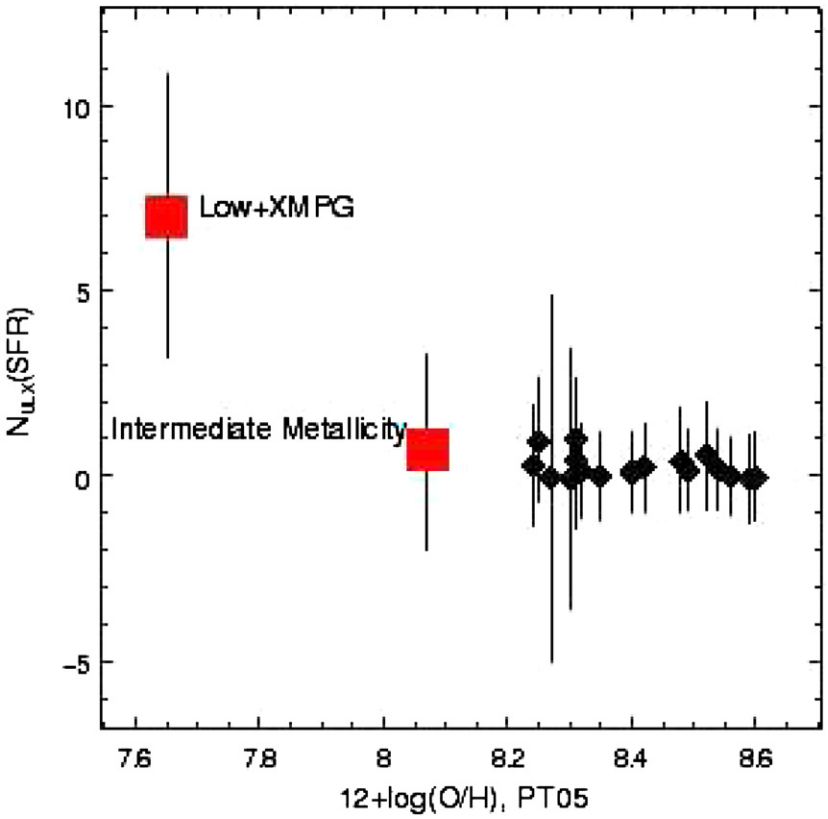


**Figure 2.** $N_{\rm ULX}$(SFR) for individual SINGS galaxies, intermediate metallicity galaxies and the combined metal poor and XMPG. This plot uses the PT05 metallicity calibration.

(A color version of this figure is available in the online journal.)

null hypothesis is that a slope does not give a statistically better fit). The *F*-test gives a significance of 0.35, confirming that a slope is not required.

Mapelli et al. (2010) use a larger sample of galaxies and find an anti-correlation between $N_{\rm ULX}$(SFR) and metallicity (their Figure 5 is directly comparable to Figure 2 of this paper). As discussed in the previous paragraph, there may be a similar trend in the SINGS galaxies but the effect is small below 12+log(O/H) = 8.0 and the scatter is large. We cannot unambiguously confirm this result. The preference for ULX to form at the low metallicities is most apparent in the lowest metallicity bin.

### *6.1. Summary and Discussion*

In this paper, we present the results of a *Chandra* survey to search for ULX in the most metal poor galaxies. We find that, compared to a comparison sample of high metallicity SINGS galaxies, the low metallicity galaxies are more likely to host a ULX. The number of ULX normalized to the SFR is ∼0.17 for the high metallicity galaxies and 7.0 for the low metallicity systems (12+log(O/H) < 8.0). The formal significance of this result is low. This study broadly agrees with the results of Mapelli et al. (2011) who also find that the number of ULX increases in lower metallicity galaxies. Mapelli et al. (2011) also claim to see a trend in the numbers of ULX as a function of metallicity. As demonstrated in Figure 2, we do not see strong evidence that $N_{\rm ULX}$(SFR) decreases as a function of metallicity above ∼8.0. This result suggests there maybe a "threshold" for more efficient ULX formation at about 12+log(O/H) < 8.

In a recent paper, we (Prestwich et al. 2012) compared the ULX population of two collisional ring galaxies, the Cartwheel and NGC 922. The Cartwheel has a relatively low metallicity (12+log(O/H) ∼ 8.1) and NGC 922 has a metallicity close to solar (12+log(O/H) ∼ 8.81). We found that the number of ULXs in NGC 922 and the Cartwheel scales with the SFR: we do not find any evidence for an excess of sources in the Cartwheel relative to NGC 922. The $N_{\rm ULX}$(SFR) values for NGC 922 and the Cartwheel are the same (within the errors) as the SINGS galaxies. This is demonstrated in Figure 3 where we plot $N_{\rm ULX}$(SFR) versus metallicity for the SINGS galaxies, the Cartwheel and NGC 922. The KK04 calibration is used for this plot as it is more appropriate for the Cartwheel and NGC 922 measurements. Figure 3 adds to the evidence that the high number of ULX in the Cartwheel is due to its very high SFR, and not a metallicity effect.

There are two hypotheses which might explain the excess of ULX in metal-poor galaxies. Linden et al. (2010) studied the effect of metallicity on HMXB production and found that the number of ULX in low metal systems increased dramatically below a threshold of $Z/Z_{\odot} < 10\%$. The high X-ray luminosities derive from Roche Lobe Overflow onto a black hole, which typically has a mass $M \leqslant 10\,M_{\odot}$. The threshold predicted by Linden et al. (2010) is consistent with the increase in $N_{\rm ULX}$(SFR) we see in galaxies with 12+log(O/H) < 8. An alternate hypothesis is that higher mass black holes are able to form in lower metallicity gas (Mapelli et al. 2009; Zampieri & Roberts 2009) leading to higher X-ray luminosities in HMXB. Our results are consistent with both of these scenarios.

Thanks to the Leigh Jenkins and the *Chandra* SINGS teams for providing results prior to publication, to Doug Swartz for giving us details of galaxies with no detected ULX and to the referee Michela Mapelli for helping to clarify many points in

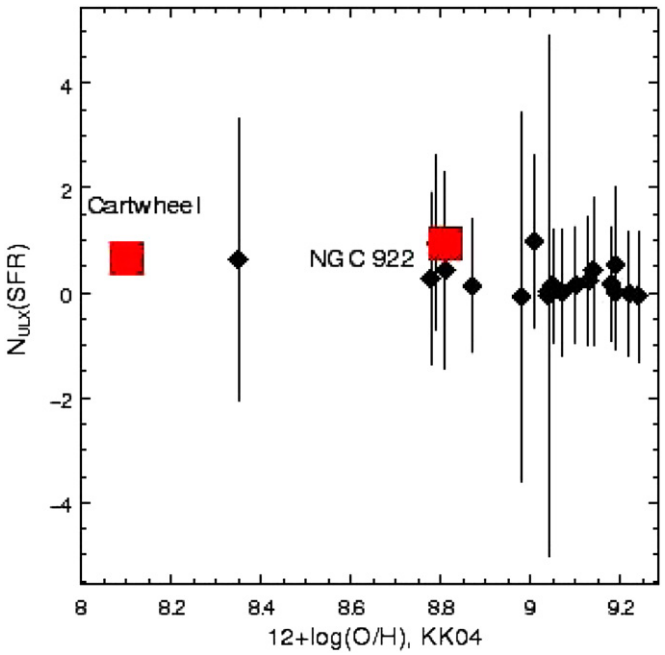


**Figure 3.** $N_{ULX}$(SFR) for individual SINGS galaxies, NGC 922 and the Cartwheel. This plot uses the KK04 metallicity calibration.

(A color version of this figure is available in the online journal.)

the paper. Support for this work was provided by the National Aeronautics and Space Administration through Chandra Award Number G0-11108A issued by the Chandra X-ray Observatory Center, which is operated by the Smithsonian Astrophysical Observatory for and on behalf of the National Aeronautics Space Administration under contract NAS8-03060. This research has made use of the NASA/IPAC Extragalactic Database (NED) which is operated by the Jet Propulsion Laboratory, California Institute of Technology, under contract with the National Aeronautics and Space Administration. Based on observations made with the NASA *Galaxy Evolution Explorer*. *GALEX* is operated for NASA by the California Institute of Technology under NASA contract NAS5-98034

## REFERENCES

Calzetti, D., Kennicutt, R. C., Engelbracht, C. W., et al. 2007, ApJ, 666, 870
Calzetti, D., Wu, S.-Y., Hong, S., et al. 2010, ApJ, 714, 1256
Colbert, E. J. M., & Mushotzky, R. F. 1999, ApJ, 519, 89
Dale, D. A., Gil de Paz, A., Gordon, K. D., et al. 2007, ApJ, 655, 863
de Vaucouleurs, G., de Vaucouleurs, A., Corwin, H. G., Jr., et al. 1991, Third Reference Catalogue of Bright Galaxies, Vol. 1–3 (Berlin: Springer)
Dickey, J. M., & Lockman, F. J. 1990, ARA&A, 28, 215
Farrell, S. A., Webb, N. A., Barret, D., Godet, O., & Rodrigues, J. M. 2009, Natur, 460, 73
Feng, H., & Soria, R. 2011, NewAR, 55, 166
Freeman, P. E., Kashyap, V., Rosner, R., & Lamb, D. Q. 2002, ApJS, 138, 185
Gehrels, N. 1986, ApJ, 303, 336
Giacconi, R., Rosati, P., Tozzi, P., et al. 2001, ApJ, 551, 624
Gladstone, J. C., Roberts, T. P., & Done, C. 2009, MNRAS, 397, 1836
Grimm, H.-J., Gilfanov, M., & Sunyaev, R. 2003, MNRAS, 339, 793
Hunter, D. A., Elmegreen, B. G., & Ludka, B. C. 2010, AJ, 139, 447
Kaaret, P., Schmitt, J., & Gorski, M. 2011, ApJ, 741, 10
Kennicutt, R. C., Jr., Armus, L., Bendo, G., et al. 2003, PASP, 115, 928
Kennicutt, R. C., Jr., Hao, C.-N., Calzetti, D., et al. 2009, ApJ, 703, 1672
Kennicutt, R. C., Jr., Lee, J. C., Funes, S. J., et al. 2008, ApJS, 178, 247
Kobulnicky, H. A., & Kewley, L. J. 2004, ApJ, 617, 240
Linden, T., Kalogera, V., Sepinsky, J. F., et al. 2010, ApJ, 725, 1984
Liu, J.-F., Bregman, J., Miller, J., & Kaaret, P. 2007, ApJ, 661, 165
Mapelli, M., Colpi, M., & Zampieri, L. 2009, MNRAS, 395, L71
Mapelli, M., Ripamonti, E., Zampieri, L., & Colpi, M. 2011, AN, 332, 414
Mapelli, M., Ripamonti, E., Zampieri, L., Colpi, M., & Bressan, A. 2010, MNRAS, 408, 234
Masters, K. 2005, PhD thesis, Cornell Univ.
Miller, M. C., & Colbert, E. J. M. 2004, IJMPD, 13, 1
Mineo, S., Gilfanov, M., & Sunyaev, R. 2012, MNRAS, 419, 2095
Moustakas, J., Kennicutt, R. C., Jr., Tremonti, C. A., et al. 2010, ApJS, 190, 233
Papaderos, P., Guseva, N. G., Izotov, Y. I., & Fricke, K. J. 2008, A&A, 491, 113
Pilyugin, L. S., & Thuan, T. X. 2005, ApJ, 631, 231
Prestwich, A. H., Galache, J. L., Linden, T., et al. 2012, ApJ, 747, 150
Ranalli, P., Comastri, A., & Setti, G. 2003, A&A, 399, 39
Roberts, T. P. 2007, Ap&SS, 311, 203
Soria, R., Cropper, M., Pakull, M., Mushotzky, R., & Wu, K. 2005, MNRAS, 356, 12
Sutton, A. D., Roberts, T. P., Walton, D. J., Gladstone, J. C., & Scott, A. E. 2012, MNRAS, 423, 1154
Swartz, D. A., Ghosh, K. K., Tennant, A. F., & Wu, K. 2004, ApJS, 154, 519
Swartz, D. A., Soria, R., & Tennant, A. F. 2008, ApJ, 684, 282
Thuan, T. X., Bauer, F. E., Papaderos, P., & Izotov, Y. I. 2004, ApJ, 606, 213
Walton, D. J., Roberts, T. P., Mateos, S., & Heard, V. 2011, MNRAS, 416, 1844
Zampieri, L., & Roberts, T. P. 2009, MNRAS, 400, 677
Zezas, A., Fabbiano, G., Baldi, A., et al. 2007, ApJ, 661, 135